Bio-Design and Manufacturing (2025) 8:581–594
https://doi.org/10.1631/bdm.2400370

RESEARCH ARTICLE

A unique bioreactor that offers synchronized physiological-like electrical and mechanical stimuli for cardiac tissue engineering

Maskit Gvirtz Markish[1] · Udi Sarig[2] · Limor Baruch[1] · Marcelle Machluf[1]

Received: 11 September 2024 / Accepted: 30 December 2024 / Published online: 23 May 2025

Abstract

Cardiac tissue engineering aims to efficiently replace or repair injured heart tissue using scaffolds, relevant cells, or their combination. While the combination of scaffolds and relevant cells holds the potential to rapidly remuscularize the heart, thereby avoiding the slow process of cell recruitment, the proper ex vivo cellularization of a scaffold poses a substantial challenge. First, proper diffusion of nutrients and oxygen should be provided to the cell-seeded scaffold. Second, to generate a functional tissue construct, cells can benefit from physiological-like conditions. To meet these challenges, we developed a modular bioreactor for the dynamic cellularization of full-thickness cardiac scaffolds under synchronized mechanical and electrical stimuli. In this unique bioreactor system, we designed a cyclic mechanical load that mimics the left ventricle volume inflation, thus achieving a steady stimulus, as well as an electrical stimulus with an action potential profile to mirror the cells' microenvironment and electrical stimuli in the heart. These mechanical and electrical stimuli were synchronized according to cardiac physiology and regulated by constant feedback. When applied to a seeded thick porcine cardiac extracellular matrix (pcECM) scaffold, these stimuli improved the proliferation of mesenchymal stem/stromal cells (MSCs) and induced the formation of a dense tissue-like structure near the scaffold's surface. Most importantly, after 35 d of cultivation, the MSCs presented the early cardiac progenitor markers Connexin-43 and α-actinin, which were absent in the control cells. Overall, this research developed a new bioreactor system for cellularizing cardiac scaffolds under cardiac-like conditions, aiming to restore a sustainable dynamic living tissue that can bear the essential cardiac excitation–contraction coupling.

Graphical abstract

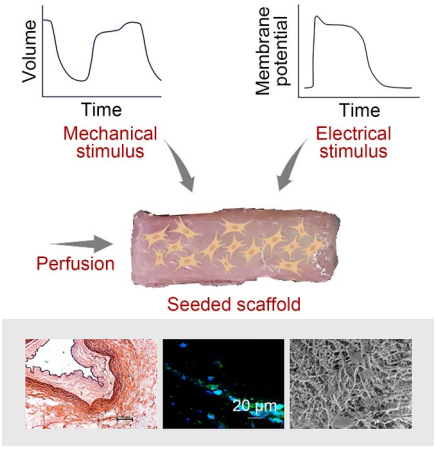

Keywords Tissue engineering · Bioreactor · Mechanical stimulation · Electrical stimulation · Perfusion · Excitation–contraction coupling · Cardiac regeneration

✉ Marcelle Machluf
machlufm@bfe.technion.ac.il

[1] Faculty of Biotechnology & Food Engineering, Technion–Israel Institute of Technology, Haifa 32000, Israel

[2] Department of Chemical Engineering, Faculty of Engineering, Ariel University, Ariel 4070000, Israel

1 Introduction

The aim of cardiac tissue engineering is to generate in vitro myocardial tissue that will offer a solution for cardiac conditions such as myocardial infarction (MI). Resulting from cardiac ischemia, MI leads to the formation of a necrotic malfunctioning tissue that interferes with cardiac contraction and electrical conductance and can lead to progressive heart failure [1]. The cardiac tissue engineering approach suggests that the necrotic area can be replaced by an engineered scaffold to halt tissue deterioration and improve cardiac function [2]. In particular, the left ventricle (LV), which endures the highest pressure within the heart and is therefore the area that is most susceptible to cardiovascular diseases, can benefit from the implantation of an engineered scaffold. The LV is also the thickest muscle within the heart; hence, its replacement with a full-thickness cellularized scaffold could restore a sustainable dynamic living tissue that would then be able to bear the essential cardiac excitation–contraction coupling [3]. Nevertheless, the design and, particularly, the proper cellularization of such a thick scaffold is challenging because of the poor nutrient and oxygen availability in its internal parts. Furthermore, previous studies have shown that, to generate a functional tissue construct, cells should be provided with an environment that mimics the physiological one [4, 5]. In our previous work, we developed a unique, custom-designed perfusion bioreactor that enabled the recellularization of a thick porcine cardiac extracellular matrix (pcECM) scaffold, thus supporting ex vivo angiogenesis and vascularization and restoring the micro- and macro-mechanical properties of the heart tissue [6–10].

In the present study, for the engineering of a functional LV construct, our goal was to provide the recellularized scaffold with a physiological-like microenvironment through cardiac-like electrical and mechanical stimulations that will facilitate a functional integration with the LV muscle.

Previous studies have demonstrated that electrical stimulation improves the cells' functional assembly and enhances cell differentiation and elongation in vitro [2, 11–13]. Using cardiomyocytes, these studies have applied an electrical stimulation designed as a rectangular wave to imitate the function of sinus atrial nodes, which activate the action potential in cardiomyocytes [11, 14–17]. Nevertheless, the transplantation of cardiomyocytes can be hindered by their high sensitivity and extremely low proliferation rate [18, 19]. Therefore, a popular alternative in cardiac cell-based regenerative therapy is the use of mesenchymal stem/stromal cells (MSCs) [20–25], due to their proliferative nature [26–29] and their potential to differentiate into cardiac-like cells [6, 30–33]. Unlike cardiomyocytes, MSCs are not triggered to create an action potential [18]; therefore, the advantages of using a rectangular wave would not be the same as those observed with cardiomyocytes. Instead, the wave shape of an action potential that mimics the electrical environment in the heart could be more beneficial. As this wave shape represents the transmembrane potential in cardiomyocytes, it generates extracellular electric fields that would be encountered by the MSCs upon scaffold transplantation [34, 35].

Mechanical stimulation has been shown to improve cell growth and enhance the synthesis of ECM, collagen, and cell proteins [30, 36, 37]. It has also been found that a simple cyclic strain mechanical stimulation [38–40] enhanced cell elongation, tissue formation, and tissue strength. Nevertheless, because the actual mechanical stimulation in the heart occurs via inflation, we hypothesized that a mechanical stimulation designed to mimic the inflation-derived shape of the LV over time can be more advantageous.

Bioreactors providing both electrical and mechanical stimulation to cell-supporting scaffolds have been introduced over the years by different groups that mostly applied uniaxial stretch-based mechanical stimuli and rectangular-shaped electrical stimuli in a static culture [41–45]. The application of these stimuli has been shown to result in diverse beneficial effects on cultured cardiomyocytes, such as increased expression of functional proteins [42, 45], cardiomyocyte maturation [41], and improved contraction [42].

However, when aiming to provide the cultured cells with both action potential-shaped electrical stimulation and physiological-like mechanical stimulation, it is particularly important to ensure these stimuli are synchronized. For such synchronization to occur in a physiological-like manner, it is essential to understand the excitation–contraction coupling in the heart. In the heart, the electrical current runs through the Purkinje fibers and triggers an action potential pulse that results in cell contraction. This does not automatically create a cardiac beat, as the accumulation of blood inside the LV prevents its compression. Instead, it causes isovolumetric contraction, which leads to an increase in pressure. Hence, the actual tissue movement will occur only later, after the aortic valve opens, leading to blood ejection and depletion from the LV and a consequent reduction in its volume. Considering the gap between cell and organ contractions, the electrical stimulation and cyclic mechanical load applied to a cellularized scaffold should be synchronized by activating the electrical stimulation at a specific time after the maximal inflation volume is reached, which is relative to the number of beats per minute [46, 47].

In the present study, our goal was to bring innovation to the field of bioreactors for cardiac tissue engineering by designing the applied stimuli and their synchronization in a more physiologically relevant manner and applying them within a perfusion bioreactor. Each of the stimuli as well as their relative start and end points was shaped to mirror the physiological environment in the heart, based on the hypothesis that cells cultured under these conditions will better

reacclimate following transplantation. User adaptability and real-time monitoring of the system are additional aspects critical for its prospective clinical application.

2 Materials and methods

2.1 Preparation of the pcECM scaffold

Thick porcine cardiac LV tissues were harvested from healthy commercial slaughter-weight pigs purchased from LAHAV C. R. O's slaughterhouse (LRI, Lahav, Israel). Decellularization was performed using our previously published protocol [10]. In brief, the LV tissues were subjected to two cycles of alternating hyper/hypotonic NaCl solutions, enzymatic treatment using trypsin (Sigma-Aldrich, USA), and detergent washes with Triton-X-100 (Merck Millipore, USA). Then, the tissue slabs (60 mm×20 mm) were sterilized using 70% ethanol and washed in phosphate-buffered saline (PBS) and culture media.

2.2 Cell culture

Bone marrow primary human MSCs (hMSCs; Lonza, Basel, Switzerland) were cultured in a humidified incubator at 37 °C with 5% CO_2 using alpha-modified Eagle's medium (α-MEM; Biological Industries, Israel) supplemented with 10% fetal calf serum (Biological Industries), 1% Pen-Strep®, 0.4% fungizone (Life Technologies, Israel), and basic fibroblast growth factor (5 ng/mL; Biological Industries). The medium was replenished every other day.

2.3 Cell seeding on acellular pcECM scaffolds

The pcECM matrices were inserted into a custom-made Teflon seeding chamber containing six wells with a length of 50 mm, width of 20 mm, and height of 37 mm. Cells were seeded at a density of 200 000 cells/cm^2, for a total of 2.4×10^6 cells seeded on top of each matrix. Following a 90-min incubation period, 20 mL of medium was added, and the matrices were incubated overnight. On the following day, the seeded matrices were transferred into culture flasks, and 60 mL of culture medium was added. The cells were labeled via pre-staining with green PKH67 (PKH67 Fluorescent cell linker kit; Sigma-Aldrich, USA) according to the manufacturer's protocol before seeding.

2.4 Cell cultivation on seeded pcECM scaffolds

Four days after cell seeding, sterile entry catheters (20 Ga, 10 cm, Single Lumen Biometrix™, Israel) were sutured to the left anterior descending coronary artery of the matrices and injected with medium to ensure a smooth perfusion flow. Another catheter was sutured to the other side of each matrix. On Day 5, some matrices were transferred to the perfusion bioreactor for dynamic cultivation, while others were left in the culture flasks to serve as controls. During the 35-d period of cultivation in the bioreactor, pH of the culture medium was monitored and glucose concentration was measured using a glucometer (FreeStyle Freedom Lite®, USA; n=3) following its validation for the complete culture medium. The Alamar Blue™ viability test was conducted according to the manufacturer's protocol (AbD Serotec, Israel; n=4).

2.5 Sterilization of the bioreactor system between subsequent experiments

Before each experiment, the bioreactor was disassembled and cleaned using water and soap, followed by washing with sodium hypochlorite. The metal screws and connectors were sonicated in a bath sonicator, and all parts were autoclaved. Then, the system was reassembled under sterile conditions. Electrodes, plastic tubing, and all non-autoclavable parts were replaced with new ones and immersed in EtOH before system assembly. The reassembled system was washed first with EtOH, then with PBS supplemented with 2% Pen-Strep® and 0.8% fungizone (Life Technologies), and finally with culture medium.

2.6 Sample fixation and analysis

After culturing, the matrices were cut and analyzed. Specifically, the samples to be subjected to fluorescence and immunofluorescence analyses were washed three times in PBS and fixed using 4% paraformaldehyde (PFA) in PBS at room temperature (RT) for 1 h. Subsequently, sterile PBS was added to dilute the solution into 2% PFA for another hour. The samples were then replenished with PBS, dried, and embedded in Tissue-Tek optimal cutting temperature (OCT) tissue embedding compound (Sakura, Torrance, USA) at RT. After 1 h, the OCT was replaced, and the molds were frozen and stored at −80 °C until use. For staining, the samples were sectioned using a cryostat (Leica CM-1900; Leica Microsystems, Germany) and mounted on positively charged glass slides (Menzel-Glaser, Germany). They were then stained for actin using Alexa Fluor™ 555 Phalloidin (Thermo Fisher Scientific, Massachusetts, USA) and immunostained for Connexin-43 (1:100, Sigma-Aldrich, #MAB3068) and α-actinin (1:200, Sigma-Aldrich, #A7811). Secondary antibodies included goat anti-mouse IgG (1:300, Sigma-Aldrich, F8521) and rabbit anti-mouse IgG (1:300, Santa Cruz, Sc45090). Counterstaining for nuclei was performed using Hoechst (Life Sciences, #H21491). For

histological analyses, samples were embedded in paraffin blocks and cross-sectioned using a microtome (Shandon Finesse 325, Microtome) prior to staining with Masson Trichrome reagent (MTC, Bio-Optica, Italy) or Hematoxylin and Eosin (H&E, Sigma-Aldrich, St Louis, MO, USA) according to the manufacturer's protocols.

2.7 Scanning electron microscopy (SEM)

The samples were submerged in PBS, mounted on aluminum stubs using tissue freezing medium (Ted Pella, Inc., AC, USA), and frozen to −25 °C using a temperature-controlled sample holder (Deben UK Ltd., Suffolk, UK). The analysis was performed using a Phenom Pro X scanning electron microscope (PhenomWorld, Eindhoven, The Netherlands), and images were captured using an accelerating voltage of 15 kV.

2.8 Fourier transform infrared (FTIR) spectroscopy

After culturing, the samples (n=3) were lyophilized and analyzed using a Thermo 6700 FTIR spectrophotometer with a smart iTR Attenuated total reflectance diamond plate at a wavelength of 500–3500 cm^{-1}. A total of 64 scans at a resolution of 4 cm^{-1} were conducted. Data were recorded and Fourier deconvoluted [48] using OMNIC™ (version 8, Thermo Scientific). The wavelength peaks were normalized by dividing each peak by each graph's area.

2.9 Statistical analysis

In each cultivation experiment, two matrices were dynamically cultivated and two other matrices were statically cultivated as controls. Each experiment was repeated at least twice, resulting in at least four replicates per group. Each analysis was repeated as indicated in each section. Statistical significance was calculated using two-way analysis of variance (ANOVA) with Tukey–Kramer's post-hoc correction, and differences were considered significant at $p<0.05$. Calculations were performed using the SAS statistical software (v. 10.0).

3 Results and discussion

In our previous work, we developed a custom-built perfusion bioreactor to support the cellularization of thick pcECMs [6, 10, 26]. Our next challenge, however, was to equip this perfusion bioreactor with synchronized mechanical and electrical stimuli that would simulate the cardiac physiological conditions, thus enabling the production of a dynamic functional living tissue.

3.1 Apparatus for the mechanical stimulation - general design

Aiming to provide the cultured cells with a mechanical stimulation that best mimicked the cardiovascular movement, we designed a mechanical load that resembled the cardiac contraction shape through the inflation of a tube that was placed under the cultured scaffold. The tube inflation was designed according to the pattern of physiological changes in the left ventricle volume (LVV) over time during cardiac contraction (Fig. 1a). To this end, a Matlab® program that acquired the known pattern of LVV variation over time was created [27, 31] for the production of a set of coordinates that were used as a traveling pattern for the linear actuator. This actuator, in turn, traveled to the appointed location and thus inflated the latex tube according to the predetermined pattern. This was achieved by inputting the coordinates into the SmartMotor Interface (SMI) software to practice as a point-by-point interval for the linear actuator (Moog Animatics, VLCT-555) governed by a servo motor (SmartMotor™ ms23165DT) that acts as the driving force, applying the mechanical load. The servo motor controls the linear actuator that is connected to four piston pumps (Metal Work, 1120250100cp) fixed to a guide unit (Metal Work, WO700502320). The linear actuator moves in and out in a cyclic manner according to the given coordinates, while the piston pumps thrust air into and out of the latex tube that is placed over a custom-made stainless-steel pipe inside the bioreactor. Consequently, the inflation and deflation of the tube precisely mimic the change in the LVV over time, mechanically stimulating the seeded matrix located above the latex tube (Fig. 1a). To avoid air loss from the system, a constant air pressure was pumped into the pistons, thus maintaining a minimum steady pressure (Fig. 1a).

3.2 Designing the coordinates for the stimulation pattern

To determine the appropriate coordinates for simulating heart contraction, an image of the LVV plotted as a function of time [31] was imported into Matlab® and converted to a matrix of values according to the color shade of each pixel. Then, this matrix was further converted to a black and white matrix (0=black, 256=white, Fig. 1b). The average location of all the white pixels in each column was calculated and inserted into an array of coordinates. All the columns with no pixels were deleted as well as the margins (Fig. 1c). The displacement array was then adapted to the desired minimum and maximum values that were determined by trial and error with the aim of reaching about 60–70 mmHg (1 mmHg=133 Pa) systolic to diastolic difference (Fig. 1d). When using approximately 120 mmHg—typical LV pressure [49]—the cells were detached from the

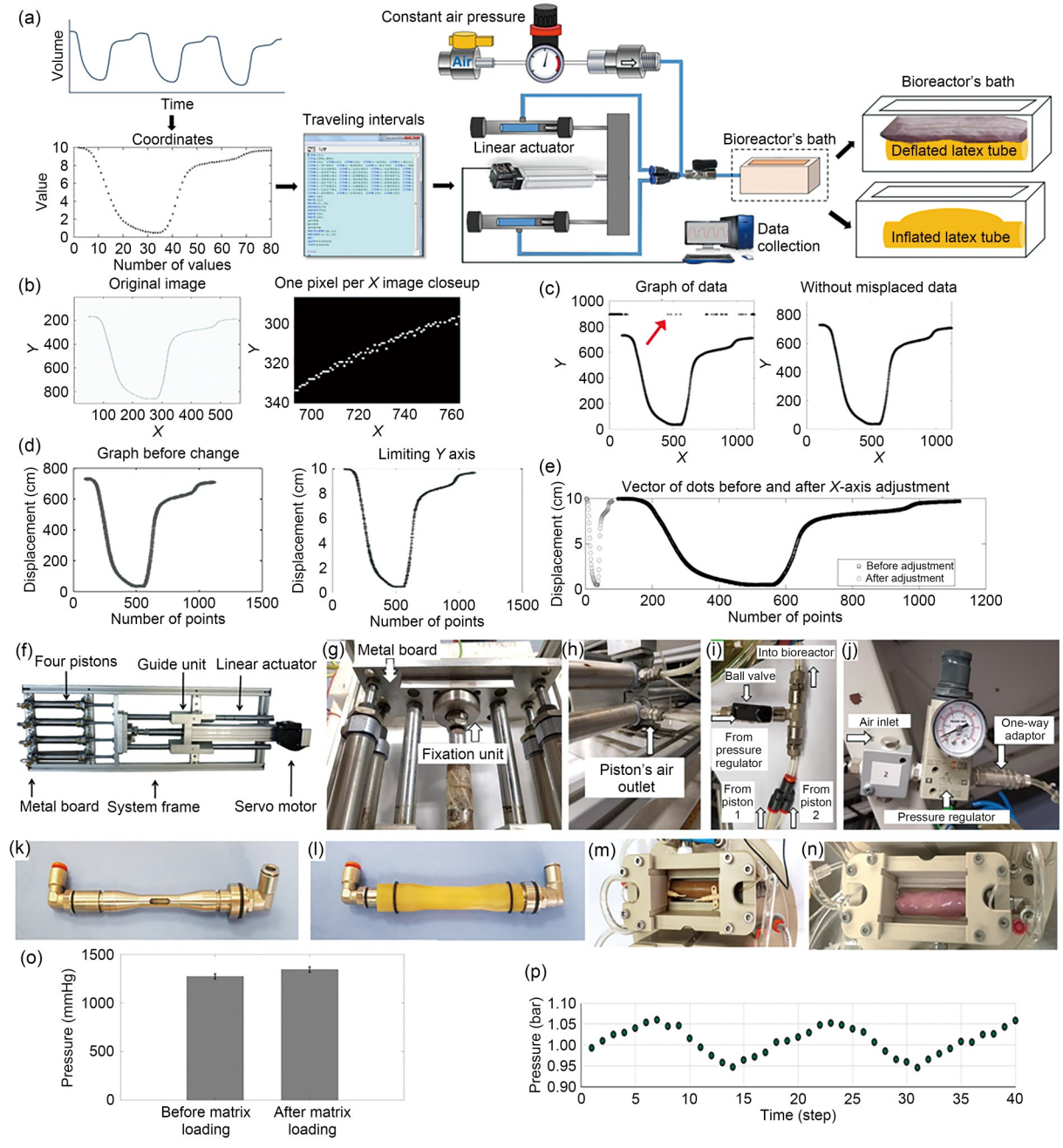

Fig. 1 Mechanical stimulus system. (a) System rationale. Graphical representation of the physiological changes in the LVV over time that were used to create a set of coordinates in Matlab®. Values were input into the designated software to create a point-by-point path that was sent to a servo motor connected to a linear actuator activating four pistons which would inflate and deflate a latex tube beneath the scaffold. Constant air pressure compensated for any air loss due to instrument deterioration. The actual volume was measured and presented in Matlab®. (b) Original image used for designing the shape of the mechanical stimulus (left) and closeup of the black and white matrix obtained from the same picture, where a single pixel corresponds to an *X* unit (right). (c) Pixel locations translated into a series of data points (left). The arrow points at misplaced data. Data series after adjusting the misplaced points (right). (d) Adjustment of the *Y* axis to displacement values corresponding to pressure values of 60–70 mmHg. On the left and right are the displacement data before and after changing the *Y* scale, respectively. (e) Adjustment of the *X* axis to serial values matching the actuator's program. (f) Image of the entire linear actuator system including a fixation unit, four pistons, and a linear actuator with a servo motor. (g) Image of the linear actuator connected via a guide unit to a metal board attached to the four pistons. (h) Image of one piston's air inlet and outlet port, through which the air is thrust into the bioreactor. (i) Image of the three-way connector, combining two pistons' external air inlets and the bioreactor's inflation system. (j) Image of the preventive air depletion system, including a pressure regulator and a one-way adaptor that allows for maintaining the cyclic stimulation pattern. (k) Image of the custom-made stainless-steel tube for the inflation/deflation device. (l) Image of the latex tube with O-rings that are wrapped around the stainless-steel tube. (m) Image of the latex tube placed into the bioreactor bath. (n) Image of the matrix fixed at both sides that is placed above the latex tube. (o) Measured pressure change in the latex tube before and after inserting the matrix (data are expressed as mean±standard deviation, n=4). (p) Measured pressure received from the pressure gauge maintains its applied shape from the piston pump. 1 mmHg=133 Pa; 1 bar=100 kPa

matrix. Therefore, the pressure was adjusted to 60–70 mmHg, which is the maximal pressure allowing cell culture.

Next, the *X* axis was converted from time in milliseconds toward serial values matching the actuator's program (Fig. 1e). Finally, the acceleration and velocity data were examined to determine the suitability of the coordinates according to the motor specifications, and the curve was smoothed to avoid stagnation of the actuator. Consequently, the program resulted in two columns (corresponding to the *X* and *Y* coordinates) representing the number of coordinates and the position at a $\Delta t{\cdot}x$ time, respectively, with Δt being determined using the SMI software according to the desired heartbeat rhythm.

3.3 Converting the pattern into inflation and deflation

To translate the linear actuator's movement into an inflating/deflating force, the linear actuator was connected to a fixation unit that facilitated the thrusting of a metal board attached to the rods of the four fixed pneumatic pistons, one for each side of the actuator (Figs. 1f and 1g), making it the center of mass. Once the linear actuator rod entered the actuator, the pistons were pressed, compressing the trapped air inside, which consequently escaped through a plastic tube connected to the pistons' inlet/outlet port (Fig. 1h). The air that exits from each pair of antagonistic tubes was joined together to increase the entrapped air volume through a micro ball valve that is then used to fill the pistons with air or empty them while maintaining the equilibrium of moments (Fig. 1i). The other side of the plastic tube was connected to a spindle filter, which sterilized the air entering the latex tube in the bioreactor. When the linear actuator's rod exits the actuator, it pulls the rods of the four pistons, which draw the air out of the latex tube back into the pistons. To avoid air losses from the inflation system over time, air was constantly supplied through a pressure regulator that kept the system at its minimum pressure value (Fig. 1j). The pressure regulator was connected to a one-way adaptor, allowing air supply while blocking leaks and maintaining a steady state of the tube's inflation–deflation cycle.

3.4 Inflation device

The latex tube was inflated by placing it around a stainless-steel hollow tube with centrally located air inlet O-rings (Figs. 1k and 1l). This device was located within the bioreactor's bath (Fig. 1m), and the matrix was placed above the latex tube, with its margins affixed to the bath so as to be stretched according to the tube inflation pattern (Fig. 1n).

3.5 Total pressure applied on the matrices

To monitor the pressure applied on the matrices, pressure measurements were taken before and after fixing the matrices in the bioreactor. These data were interpolated in Matlab® to extract the maximum pressure values, calculate the difference between averages, and convert them into mmHg. The results indicated that the matrices endured a pressure of ΔP=69.83 mmHg (Fig. 1o). Furthermore, pressure was constantly measured during these experiments using a pressure gauge, and the acquired data resulted in a steady state pressure curve, indicating that no air was depleted over time and that the LVV pattern was successfully preserved (Fig. 1p).

3.6 Apparatus for electrical stimulation

In the heart, cardiomyocytes are given a sinus current to reach a threshold that triggers an action potential, leading to cell contraction. Previous cardiac tissue engineering studies have demonstrated that electrical stimulation also affects cells in vitro by improving their functional assembly while enhancing cell differentiation and elongation [12]. In these studies, a rectangular electrical wave was used to mimic the function of the sinus atrial nodes, thus activating the action potential [14, 15]. This waveform is highly beneficial when working with cardiomyocytes. Nevertheless, when culturing MSCs as a cell model for cardiac tissue engineering [20–25], their inability to be triggered and create an action potential [18] should be considered. Therefore, in the present study, to mimic the electrical environment that these cells would experience in the heart following transplantation, an action potential-like waveform was chosen for their in vitro stimulation. This waveform comprised three phases in the following order: a fast increase in the membrane potential (depolarization phase), a plateau phase, and a final repolarization phase (Fig. 2a) [50].

To apply the electrical stimulation, we designed a system in which an electrical signal created by a computer was converted into an analog signal that stimulated the scaffold and its residing cells using a set of two parallel platinum electrodes (Fig. 2a).

To create an action potential-shaped signal, we used the same Matlab® program that was used to create the mechanical LVV-shaped stimulation coordinates. An action potential waveform plot of voltage versus time was translated into coordinates and adjusted to a predetermined amplitude and number of coordinates (Fig. 2b). The program output included three electrical signals, the first two of which were transferred to the bioreactor baths, while the third was transferred to the analog-to-digital converter (National Instruments, NI-9269) and returned to the software for feedback and monitoring. Thus, a sample of 5000 values

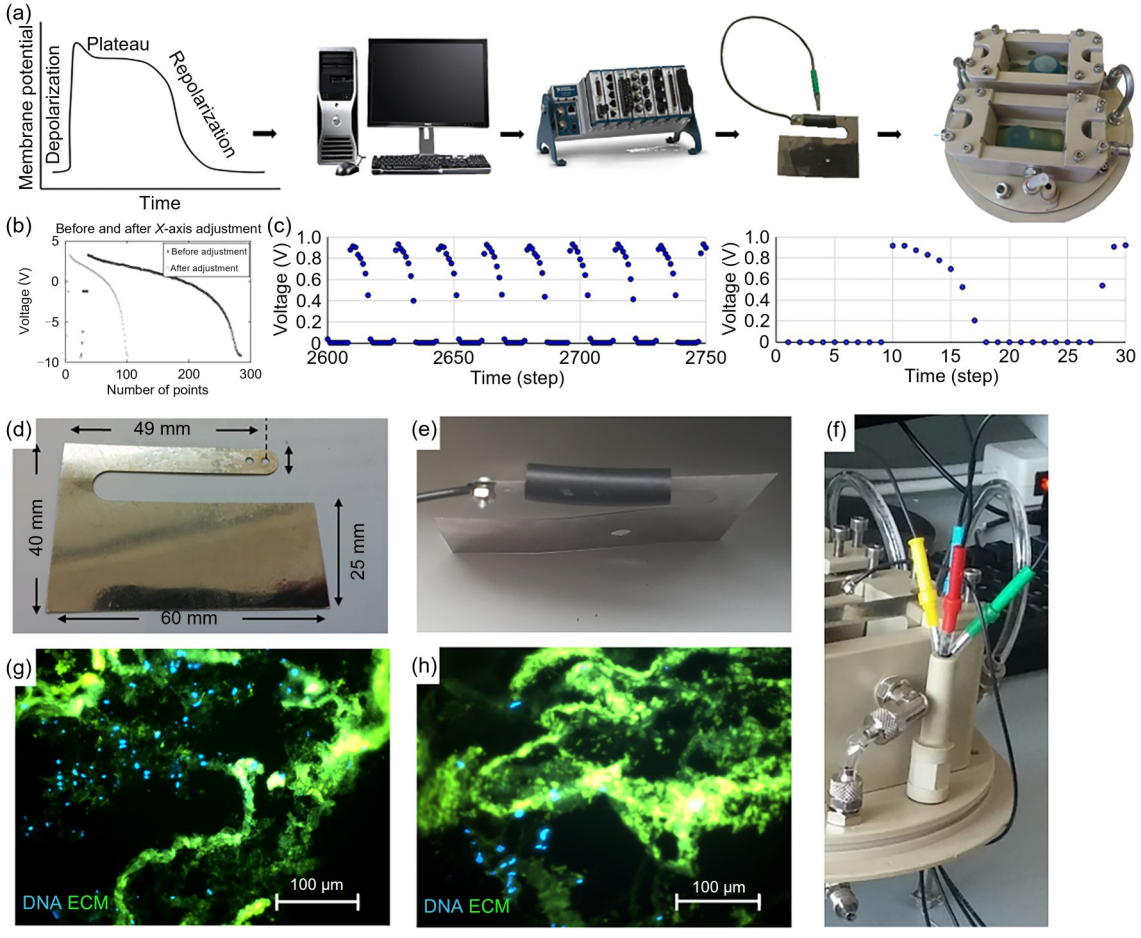

Fig. 2 Electrical stimulus system. (a) Design of the system for electrical stimulation. The action potential wave-shaped pulse was created using LabVIEW and transferred through an NI digital-to-analog converter to electrically stimulate the matrix with platinum foil electrodes placed within the bioreactor. (b) Results of the action potential from the written Matlab software after translating the image pixels to data points, adjusting the *Y* scale according to the predefined voltage values, and applying the smooth function. Values are shown before and after the adjustment of the *X* axis. (c) Electrical signals obtained at ±30 min (left) and ±30 s (right) of measurements showing stability over time and the preservation of the voltage waveform that reached the electrodes. (d) Image of an electrode. (e) Image of the tin-plated copper wire connected via a screw before ironing the heat-shrink sleeve. (f) Images of the banana plug connectors and the bioreactor's hollow pole allowing the transfer of electricity from a sterile environment to the outside of the bioreactor. (g, h) Representative images of cells cultured under electrical stimulation obtained via confocal microscopy: electrically stimulated matrix (g) and control non-stimulated matrix (h). The green and blue colors denote the matrix (autofluorescence) and the cells' nuclei (DAPI), respectively. DAPI: 4',6-diamidino-2-phenylindole

from the electrical stimulation feedback was recorded every hour to ensure proper system maintenance. The collected data reflected a steady electrical current with minimal reduction that also preserved the action potential shape (Fig. 2c).

3.7 Electrode design

The electrodes were produced from platinum (99.95%, Goodfellow, Germany) using electrical discharge machining (Harpaz Industries, Israel). A rectangle of 60 mm× 25 mm×0.1 mm was added with an L-shaped section at one side of the electrode (Fig. 2d). The electrodes were connected to tin-plated copper wires (NTE Electronics, Inc., USA) using 2-mm screws and covered with heat-shrink tubes to avoid corrosion (Fig. 2e). The wires were then connected through a hollow pole in the perfusion bioreactor to allow the association of sterile parts with the outer environment (Fig. 2f). On the other side, the wires were connected to the analog output system for data acquisition.

3.8 Electrical stimulation supports cell culture

Previous studies demonstrating the beneficial effect of electrical stimulation on cultured cells have applied voltages ranging between 2 V and 50 V per cm of electrode distance [51]. Nevertheless, the rectangular waveform was only applied for 1–5 ms [52–54], while the action potential duration was 350 ms [55]. Therefore, to apply an action

potential-like stimulus for 350 ms, it was necessary to use an electrical stimulus at a lower voltage to avoid cellular damage [5, 48]. Accordingly, an amplitude of −9 to 4 V was used at 80 beats per minute (BPM), which is equivalent to 1.33 Hz. To rule out any negative effect of the designed electrical stimulus on the cells, thick pcECM scaffolds were seeded with MSCs and cultured. The seeded scaffolds were cultivated for 14 d without stimulation and then subjected to the designed electrical stimulus, but without perfusion, in order to isolate their effect. The control groups were not subjected to any electrical stimulus. After 7 d, the samples were fixed and the cell nuclei were stained with 4',6-diamidino-2-phenylindole (DAPI), which contrasted the green autofluorescence of the pcECM matrix [56], thus confirming the presence of cells on both the electrically stimulated scaffolds (Fig. 2g) and on the non-stimulated control (Fig. 2h).

3.9 Synchronization of the designed mechanical and electrical stimuli

The two types of stimuli were synchronized with the aim of optimally replicating the cardiac physiological conditions. In the heart, the LVV reaches two extremum values, i.e., the maximum value, which is obtained immediately after the action potential increases, and the minimum value, which is obtained following the entire action potential cycle, as previously described in the Wiggers diagram [57]. Hence, the excitation–contraction coupling in the heart is a matter of cause and effect. The cells' action potential causes the contraction of single cells. Numerous contracting cells apply pressure on the cardiac tissue toward contraction, which, however, is resisted by the blood within the heart as well as the entire vascular system, resulting in the volume barely changing as pressure increases. Eventually, the pressure is sufficiently high to open the aortic valve that allows contraction and the reduction of the cardiac LVV.

When designing the synchronization between the stimuli in our bioreactor, it was decided to replace the cause and effect of the physiological system. This was done because the designed electrical stimulation is more easily manipulated and immediately responsive, while the mechanical system is more robust and delayed by friction.

Hence, a pressure follow-up curve was used to define the timing for the initiation of the electrical stimuli. A pressure gauge (ADZ–SML 10.0, ADZ Nagano Sensortechnik) was connected to the bioreactor's latex tube outlet to constantly measure the pressure applied on the matrix. The pressure data were acquired using a LabVIEW program, through which they were filtered and converted to bar units (1 bar=100 kPa). Real-time extremum values were then used to trigger the cue for commencing the electrical stimulation process (Fig. 3a). A time suspension mechanism was set to enable the control of the time gap between the LVV waveform maximum and the start of the action potential waveform by adding a user-defined number of electrical resting voltages, thus adjusting the delay to mimic human physiology (Figs. 3b and 3c).

3.10 System monitoring and validation

During cultivation, the LabVIEW software was programmed to acquire useful data such as the BPM, which measured the time between two maximum pressure values and allowed the maintenance of the desired physiological rhythm (60 BPM in our study, Fig. 3b). Data were also acquired for an indicator termed "maximum pressure array," which added the maximum pressure value of each inflation cycle to an array of values, demonstrating the stability of tube inflation over time (Fig. 3c). To enable the conduction of long-term studies, it was necessary to address challenges such as material deterioration, sterility maintenance, and potential operational mistakes. To this end, high-tolerance materials were selected, processes were constantly monitored, and careful practice of sterile procedures was implemented. Furthermore, several measures were taken at the design level to monitor and validate the proper system operation. First, to prevent system damage resulting from mistakenly connecting opposite electrical wires, the pressure gauge circuit was designed to include a safety diode protecting the current direction (Fig. 3d). Second, a light indicator of the power supply and an on/off switch were installed in the pressure system power supply. An additional challenge was to use a single pressure gauge for parallel experiments. For this purpose, a ball valve connector was installed, ensuring a clear path from one inflating tube while blocking the other, thus allowing user control of the experiment. Moreover, to avoid wire entanglement, a plugin connector was fitted (Fig. 3d). Finally, the mechanical pressure and electrical signals obtained from the pressure gauge as well as the electrical feedback path were displayed in real time, side by side, to verify that both signals were synchronized in a way that mimicked physiological conditions [50] (Fig. 3e).

3.11 Scaffold recellularization using our designed bioreactor

The efficiency of the stimulated perfusion bioreactor for scaffold cellularization was ultimately assessed. Cells were seeded on a full-thickness vascularized ECM scaffold, and after 5 d of cultivation (Day 0), the scaffolds were transferred to the perfusion bioreactor under synchronized mechanical (frequency: 1 Hz; pressure: 1.1 bar) and electrical (amplitude: 0–1 V; duration: 312.5 ms) stimulation.

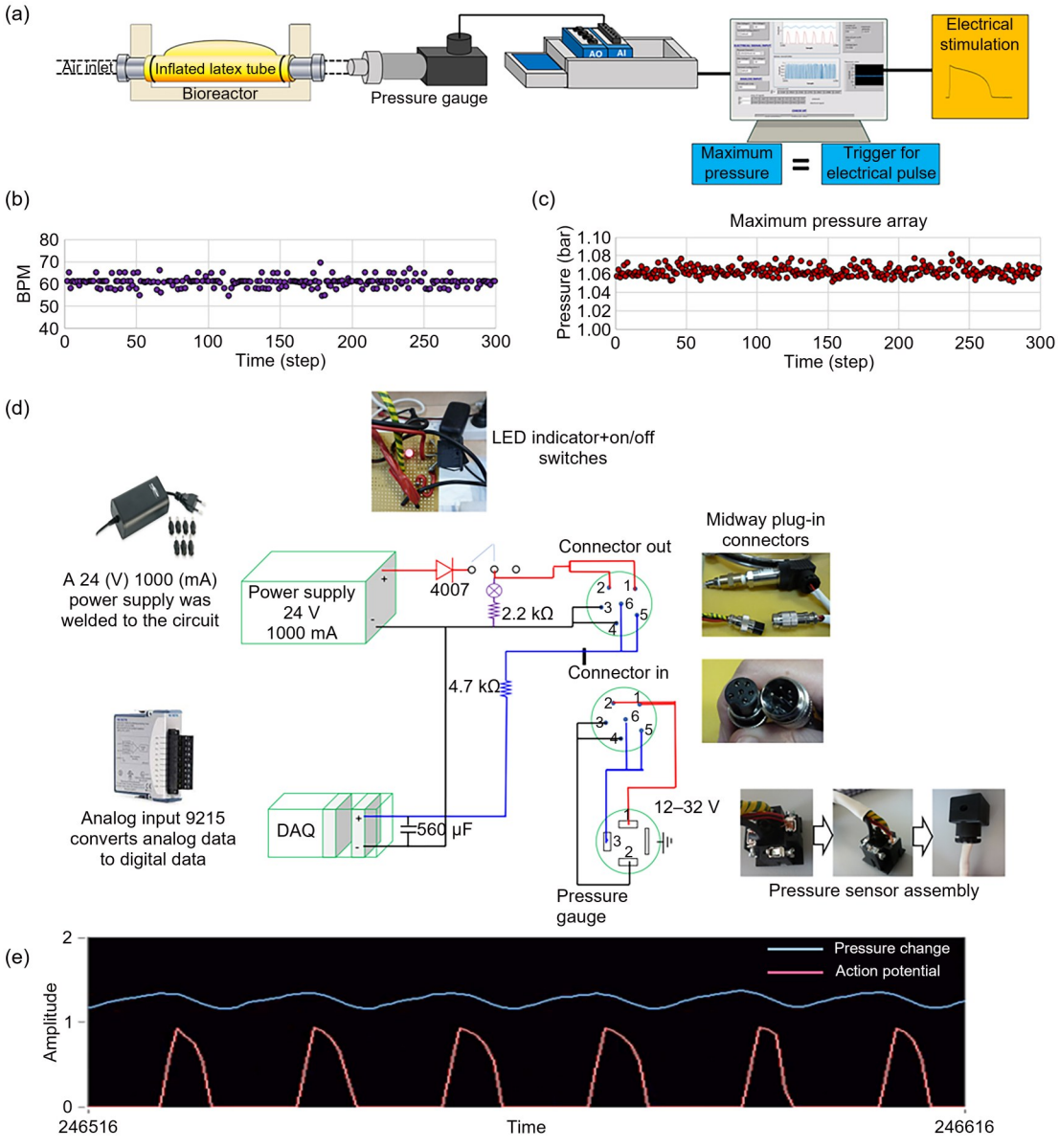

Fig. 3 Synchronization of the mechanical and electrical stimuli. (a) Scheme of the synchronization system. After the air inflates the latex tube, a pressure gauge connected to the other end of the tube transforms the pressure in bars into analog voltages ranging from 0 to 10 V. Subsequently, a data acquisition device converts the analog voltages into digital data, which are imported into LabVIEW software and filtered. In this software, the maximum values are then used to trigger a time suspension followed by an electrical signal shaped as an action potential that is applied on the tissue inside the bioreactor. (b) Beats per minute (BPM, measured by the system over time) showing a steady mechanical stimulation, with computer-based recognition of every beat. (c) Maximum pressure values as identified by the pressure gauge for each recognized step, thus verifying the system's steady state. (d) Scheme of the monitoring and validation system: a power supply was connected to the pressure transmitter alongside a data acquisition instrument; the system included a plugin/out and an indication diode. (e) Graphs of the synchronized stimuli over time. LED: light emitting diode. 1 bar=100 kPa

As shown in Fig. 4a, the steady state of glucose consumption confirmed that the stimulated culture and the control were free of contamination. Similarly, the pH measurements indicated proper culture conditions (Fig. 4b). A follow-up assay of cell viability showed fluctuations in viability levels in both the stimulated and non-stimulated scaffolds, reflecting the natural balance between dying and proliferating cells. No differences were observed between the bioreactor-cultured scaffolds and the control scaffolds during the first week of culture in the bioreactor. Nevertheless, after 2 weeks, some differences were detected. Specifically, toward the end of the experiment, the mechanically and electrically stimulated scaffolds exhibited a higher viability level compared with the non-stimulated scaffolds (Fig. 4c), which was also seen to a lesser extent when each individual stimulus was applied (Fig. S1 in the

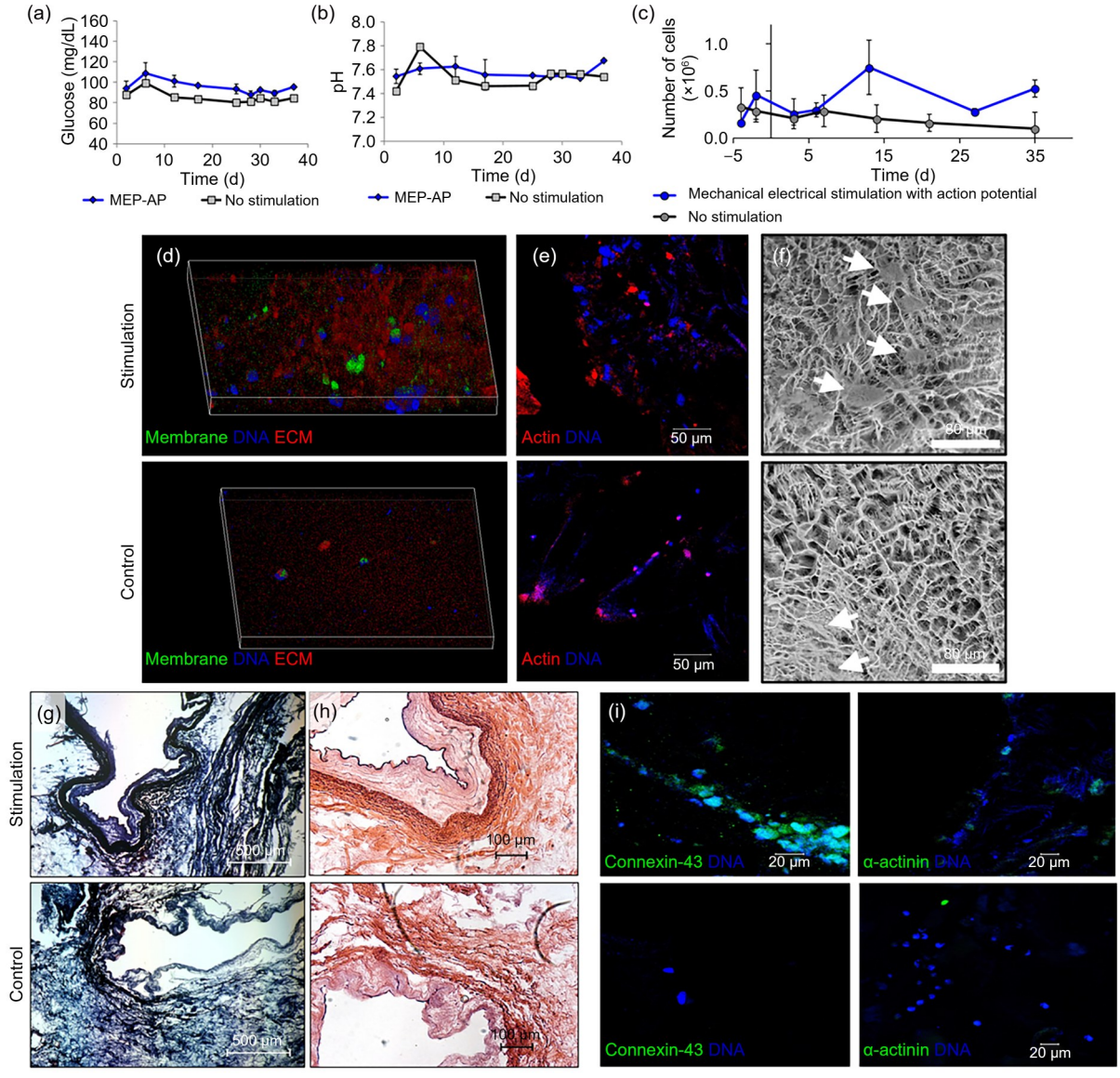

Fig. 4 Scaffold recellularization. Glucose (a) and pH (b) measurements in the media of cells cultured on the ECM matrix under synchronized mechanical and electrical stimuli in the bioreactor compared with the control. (c) Cell viability over time. (d, e) Representative confocal microscopy images of cells cultured on the ECM matrix under synchronized mechanical and electrical stimuli in the bioreactor (upper panels) compared with the control (lower panels). (d) Green, cell membranes (PKH67); blue, cell nuclei (Hoechst); red, matrix (autofluorescence). (e) Red, actin (phalloidin); blue, cell nuclei (Hoechst); scale bars: 50 μm. (f) SEM images showing the cultured MSCs on the stimulated and control ECM matrix; the arrows point at the cells. Scale bars: 80 μm. Masson trichrome (g) and H&E (h) staining of the ECM matrix cellularized under synchronized mechanical and electrical stimuli in the bioreactor (upper panels) compared with the control (lower panels). Scale bars: 500 and 100 μm, respectively. (i) Cardiac marker staining of MSCs cultured on the ECM matrix under synchronized mechanical and electrical stimuli in the bioreactor (upper panels) compared with the control (lower panels). The cardiac early markers Connexin-43 and α-actinin are indicated in green, while the cell nuclei are indicated in blue; scale bars: 20 μm. MEP-AP: mechanical and electrical stimulation. Data in (a–c) are expressed as mean±standard deviation (n=4)

supplementary information). These results imply that continuous stimulation slowly leads to a significant effect on cell proliferation, which would not be observed in short-term studies. Moreover, confocal analyses of cellularized pcECM scaffolds after 35 d of culture showed a higher cell density for scaffolds cultured under synchronized mechanical and electrical stimulation than for the non-stimulated controls (Fig. 4d). These findings were further confirmed by the results obtained from the recellularized scaffolds fluorescently stained for actin (Fig. 4e) and from SEM analyses, which demonstrated the fibrous scaffold topography supporting the cultured cells (Fig. 4f). Masson's trichrome staining (Fig. 4g) as well as H&E staining (Fig. 4h) of the recellularized scaffolds revealed that both the

stimulated and non-stimulated scaffolds were well populated. Cells were concentrated in a sparse layer on the scaffold's surface, probably due to the higher nutrient and oxygen availability. Nevertheless, the cells in the stimulated scaffolds were organized in a dense tissue-like structure, while those in the control scaffolds exhibited a looser, non-organized growth. These results are in line with previous studies showing that short-term dual stimulation for 2–4 d (including unsynchronized co-stimulations and different amplitude shapes) promotes cell repopulation and viability as well as positive tissue remodeling [44].

To preliminarily assess the fate of the cultured cells, immunofluorescent staining analyses were performed for the early cardiac progenitor markers Connexin-43 and α-actinin, whose expression was observed in the stimulated cells but not in the control matrices (Fig. 4i). Notably, Connexin-43 was not located at the interface of adjacent cells, most likely due to the cells' immature stage or to the insufficient cell density disabling such an interface. These results were in line with previously published research showing that the cardiac microenvironment provided to the cells using electrical and mechanical stimulation or even by the presence of cardiomyocytes promotes MSC differentiation toward cardiac-like cells [58–61]. Nevertheless, the application of both electrical and mechanical stimuli that are synchronized based on a physiological-like timing on MSCs has not been published before, and our findings can thus lead to a new promising approach for cardiac tissue engineering.

3.12 Effect of culture conditions in the bioreactor on the scaffolds' molecular structure

Previous studies have suggested that electrical stimulation induces ECM deterioration due to excessive voltage [62, 63], while mechanical stimulation causes ruptures due to overload if applied for long periods [30]. To address the impairment of recellularized pcECM scaffolds, a comparative analysis of stimulated and non-stimulated scaffolds was conducted via FTIR spectroscopy (Fig. 5a), and the protein secondary structures were quantified using Fourier self-deconvolution (Figs. 5b and 5c). The comparison between the stimulated and control scaffolds revealed that the secondary structures of random coil, β-sheet, and α-helix maintained their original relative quantity in the matrices, while the relative quantity of β-turn and other structures significantly differed (Fig. 5c, $p<0.05$). Nonetheless, as observed in the Fourier self-deconvolution curves, the β-sheet and random coil structures are very close in the wavelength absorbance, and at least some of the differences may be due to

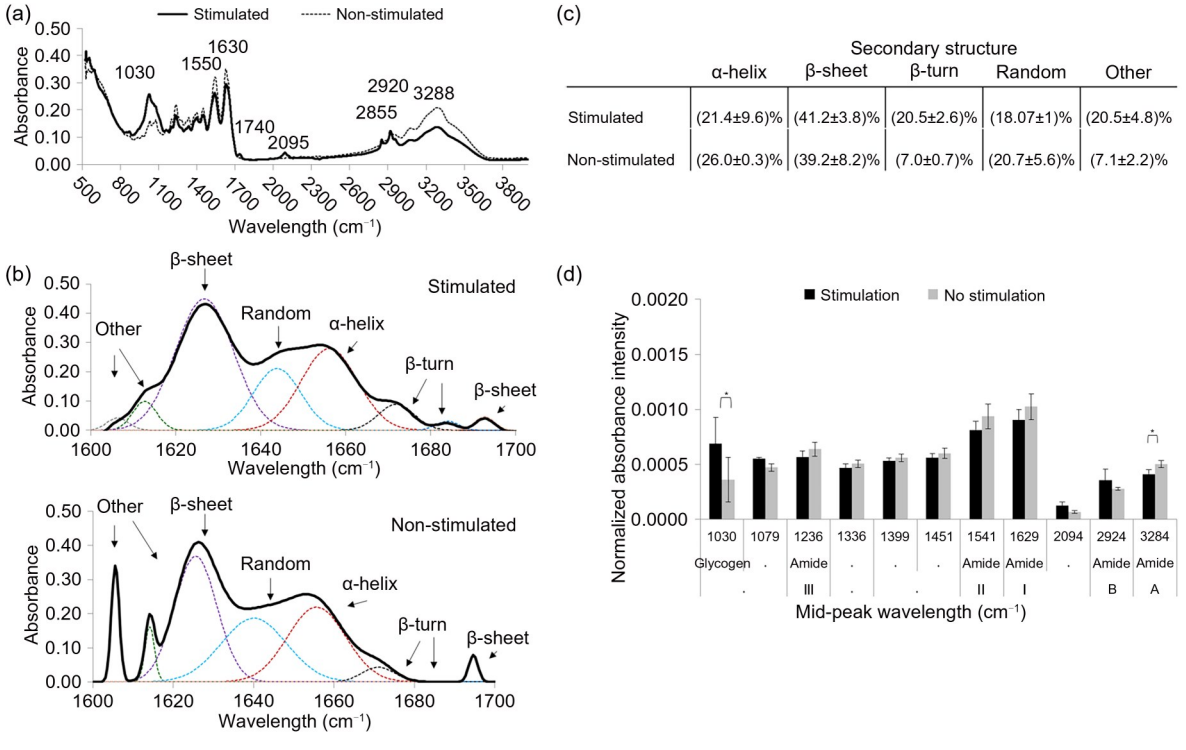

Fig. 5 Molecular structure of the scaffolds. (a) FTIR analysis of the ECM matrices cellularized under synchronized mechanical and electrical stimuli in the bioreactor compared with the non-stimulated control. (b) Deconvolution of the FTIR spectra to determine the protein secondary structures. (c) Table summarizing the relative amounts of protein secondary structures quantified from the FTIR deconvolution graphs. (d) Peaks of the FTIR spectra extracted and normalized by graph area; each peak indicates the amount of a certain chemical bond or material within the cellularized matrices. Data are expressed as mean±standard deviation (n=3). $^{*}p<0.05$

very small shifts in the ECM structures. In terms of the presence of different bonds, our results showed a decrease in amide A (3284 cm^{-1}) in the stimulated matrices but no differences in amide B (2924 cm^{-1}) or in the main collagen fingerprint bonds (amide I (1630 cm^{-1}), amide II (1539 cm^{-1}), and amide III (1231 cm^{-1})). Glycogen levels (1030 cm^{-1}) [64, 65] were shown to increase in the stimulated matrices (Fig. 5d). Overall, while the stimulated matrix conserved most of its structures, some of them were modified, potentially due to the stimulation itself but also to the higher numbers of populating cells.

4 Conclusions

In the present study, a modular system was developed for the dynamic cellularization of thick cardiac scaffolds under mechanical and electrical stimuli. The system was designed with user adaptability for the selection of the shape, type, intensity, and frequency of each stimulus while maintaining a highly sterile environment. A cyclic mechanical load that mimics the left ventricle volume inflation was successfully designed, achieving a steady stimulus over a period of at least 35 d. Moreover, the electrical stimulus was designed to have an action potential profile mimicking the microenvironment of cells in the heart tissue. Finally, the mechanical load and electrical stimulation were synchronized according to cardiac physiology, with constant regulatory feedback. These synchronized stimuli provided an improved proliferative profile for MSCs that were cultivated on thick pcECM scaffolds. Such cell proliferation resulted in a dense tissue-like structure near the scaffold's surface. Notably, after 35 d of cultivation in the designed bioreactor under stimulation (and without any additional chemical stimulation), the cells presented early cardiac markers that were not detectable in the control. Overall, our research offers a validated bioreactor system that mimics the physiological conditions of the heart, supports cell proliferation, and directs cellular differentiation toward cardiac-like cells. This system opens new possibilities for tissue engineering researchers in cellularizing different types of cardiac scaffolds prior to their transplantation, thus potentially generating a more functional graft. Furthermore, the adaptability of this system enables the optimization of each stimulus according to the studied scaffold and seeded cells. This bioreactor system, relying on the controllable physiological-like environment, can also be used for ex vivo research of the heart under different cardiac conditions and corresponding treatments.

Supplementary Information The online version contains supplementary material available at https://doi.org/10.1631/bdm.2400370.

Acknowledgements This research was funded by the Israeli Ministry of Innovation, Science and Technology (Grant No. 3-11873), the Israel Science Foundation (Grant No. 1563/10), the Randy L. and Melvin R. Berlin Family Research Center for Regenerative Medicine, and the Gurwin Family Foundation.

Author contributions MM conceived, designed, and supervised the research. MGM performed the research with the help and consultation of US. MGM, LB, and MM analyzed and interpreted the data. LB, MGM, and MM prepared the manuscript.

Funding Open access funding provided by Technion–Israel Institute of Technology.

Declarations

Conflict of interest The authors declare that they have no conflict of interest.

Ethical approval This work does not contain any studies with human or animal subjects performed by any of the authors. Porcine tissues were purchased from LRI (Lahav, Israel) in accordance with the Israeli Animal Welfare (Protection and Experimentation) Law and supervised by the regulatory Israeli National Ethics Committee.

Data availability The data that support the findings of this study are available from the corresponding author upon reasonable request.

References

1. Bahit MC, Kochar A, Granger CB (2018) Post-myocardial infarction heart failure. JACC Heart Fail 6(3):179–186. https://doi.org/10.1016/j.jchf.2017.09.015
2. Tadevosyan K, Iglesias-García O, Mazo MM et al (2021) Engineering and assessing cardiac tissue complexity. Int J Mol Sci 22(3):1479. https://doi.org/10.3390/ijms22031479
3. Patterson T, Rivolo S, Burkhoff D et al (2021) Impact of coronary artery disease on contractile function and ventricular-arterial coupling during exercise: simultaneous assessment of left-ventricular pressure-volume and coronary pressure and flow during cardiac catheterization. Physiol Rep 9(10):e14768. https://doi.org/10.14814/phy2.14768
4. Moysidou CM, Barberio C, Owens RM (2021) Advances in engineering human tissue models. Front Bioeng Biotechnol 8: 620962. https://doi.org/10.3389/fbioe.2020.620962
5. Simon LR, Masters KS (2020) Disease-inspired tissue engineering: investigation of cardiovascular pathologies. ACS Biomater Sci Eng 6(5):2518–2532. https://doi.org/10.1021/acsbiomaterials.9b01067
6. Sarig U, Nguyen EB, Wang Y et al (2015) Pushing the envelope

in tissue engineering: ex vivo production of thick vascularized cardiac extracellular matrix constructs. Tissue Eng Part A 21(9–10):1507–1519. https://doi.org/10.1089/ten.tea.2014.0477
7. Bronshtein T, Au-Yeung GCT, Sarig U et al (2013) A mathematical model for analyzing the elasticity, viscosity, and failure of soft tissue: comparison of native and decellularized porcine cardiac extracellular matrix for tissue engineering. Tissue Eng Part C Methods 19(8):620–630. https://doi.org/10.1089/ten.TEC.2012.0387
8. Sarig U, Sarig H, Gora A et al (2018) Biological and mechanical interplay at the macro- and microscales modulates the cell-niche fate. Sci Rep 8:3937. https://doi.org/10.1038/s41598-018-21860-6
9. Au-Yeung GCT, Sarig U, Sarig H et al (2017) Restoring the biophysical properties of decellularized patches through recellularization. Biomater Sci 5(6):1183–1194. https://doi.org/10.1039/c7bm00208d
10. Sarig U, Au-Yeung GCT, Wang Y et al (2012) Thick acellular heart extracellular matrix with inherent vasculature: a potential platform for myocardial tissue regeneration. Tissue Eng Part A 18(19–20):2125–2137. https://doi.org/10.1089/ten.TEA.2011.0586
11. Radisic M, Park H, Shing H et al (2004) Functional assembly of engineered myocardium by electrical stimulation of cardiac myocytes cultured on scaffolds. Proc Natl Acad Sci USA 101(52):18129–18134. https://doi.org/10.1073/pnas.0407817101
12. Tandon N, Marsano A, Cannizzaro C et al (2008) Design of electrical stimulation bioreactors for cardiac tissue engineering. In: 30th Annual International Conference of the IEEE Engineering in Medicine and Biology Society, p.3594–3597. https://doi.org/10.1109/IEMBS.2008.4649983
13. Lim D, Renteria ES, Sime DS et al (2022) Bioreactor design and validation for manufacturing strategies in tissue engineering. Bio-Des Manuf 5(1):43–63. https://doi.org/10.1007/s42242-021-00154-3
14. Barash Y, Dvir T, Tandeitnik P et al (2010) Electric field stimulation integrated into perfusion bioreactor for cardiac tissue engineering. Tissue Eng Part C Methods 16(6):1417–1426. https://doi.org/10.1089/ten.TEC.2010.0068
15. Maidhof R, Tandon N, Lee EJ et al (2012) Biomimetic perfusion and electrical stimulation applied in concert improved the assembly of engineered cardiac tissue. J Tissue Eng Regen Med 6(10):e12–e23. https://doi.org/10.1002/term.525
16. Tandon N, Marsano A, Maidhof R et al (2011) Optimization of electrical stimulation parameters for cardiac tissue engineering. J Tissue Eng Regen Med 5(6):e115–e125. https://doi.org/10.1002/term.377
17. Carrier RL, Papadaki M, Rupnick M et al (1999) Cardiac tissue engineering: cell seeding, cultivation parameters, and tissue construct characterization. Biotechnol Bioeng 64(5):580–589. https://doi.org/10.1002/(SICI)1097-0290(19990905)64:5<580::AID-BIT8>3.0.CO;2-X
18. Li GR, Sun HY, Deng XL et al (2005) Characterization of ionic currents in human mesenchymal stem cells from bone marrow. Stem Cells 23(3):371–382. https://doi.org/10.1634/stemcells.2004-0213
19. Taylor DA (2004) Cell-based myocardial repair: how should we proceed? Int J Cardiol 95:S8–S12. https://doi.org/10.1016/s0167-5273(04)90003-4
20. Zhang JF, Wu YC, Chen AQ et al (2015) Mesenchymal stem cells promote cardiac muscle repair via enhanced neovascularization. Cell Physiol Biochem 35(3):1219–1229. https://doi.org/10.1159/000373945
21. Karantalis V, Hare JM (2015) Use of mesenchymal stem cells for therapy of cardiac disease. Circ Res 116(8):1413–1430. https://doi.org/10.1161/CIRCRESAHA.116.303614
22. Alestalo K, Lehtonen S, Yannopoulos F et al (2013) Activity of mesenchymal stem cells in a nonperfused cardiac explant model. Tissue Eng Part A 19(9–10):1122–1131. https://doi.org/10.1089/ten.TEA.2012.0241
23. Fukuda K (2003) Regeneration of cardiomyocytes from bone marrow: use of mesenchymal stem cell for cardiovascular tissue engineering. Cytotechnology 41(2–3):165–175. https://doi.org/10.1023/A:1024882908173
24. Paez-Mayorga J, Hernández-Vargas G, Ruiz-Esparza GU et al (2019) Bioreactors for cardiac tissue engineering. Adv Healthc Mater 8(7):e1701504. https://doi.org/10.1002/adhm.201701504
25. Singh A, Singh A, Sen D (2016) Mesenchymal stem cells in cardiac regeneration: a detailed progress report of the last 6 years (2010-2015). Stem Cell Res Ther 7(1):82. https://doi.org/10.1186/s13287-016-0341-0
26. Eitan Y, Sarig U, Dahan N et al (2010) Acellular cardiac extracellular matrix as a scaffold for tissue engineering: in vitro cell support, remodeling, and biocompatibility. Tissue Eng Part C Methods 16(4):671–683. https://doi.org/10.1089/ten.TEC.2009.0111
27. Dodge HT (1968) Functional characteristics of the left ventricle in heart disease. Ann Intern Med 69(5):941–948. https://doi.org/10.7326/0003-4819-69-5-941
28. Wen ZZ, Zheng SX, Zhou CQ et al (2011) Repair mechanisms of bone marrow mesenchymal stem cells in myocardial infarction. J Cell Mol Med 15(5):1032–1043. https://doi.org/10.1111/j.1582-4934.2010.01255.x
29. Lin XL, Peng P, Cheng L et al (2012) A natural compound induced cardiogenic differentiation of endogenous MSCs for repair of infarcted heart. Differentiation 83(1):1–9. https://doi.org/10.1016/j.diff.2011.09.001
30. Shachar M, Benishti N, Cohen S (2012) Effects of mechanical stimulation induced by compression and medium perfusion on cardiac tissue engineering. Biotechnol Prog 28(6):1551–1559. https://doi.org/10.1002/btpr.1633
31. Pedrizzetti G, Perktold K (2003) Cardiovascular Fluid Mechanics (1st Ed.). Springer, Vienna, Austria. https://doi.org/10.1007/978-3-7091-2542-7
32. Zhao JJ, Liu XC, Kong F et al (2014) Bone marrow mesenchymal stem cells improve myocardial function in a swine model of acute myocardial infarction. Mol Med Rep 10(3):1448–1454. https://doi.org/10.3892/mmr.2014.2378
33. Rahbarghazi R, Nassiri SM, Ahmadi SH et al (2014) Dynamic induction of pro-angiogenic milieu after transplantation of marrow-derived mesenchymal stem cells in experimental myocardial infarction. Int J Cardiol 173(3):453–466. https://doi.org/10.1016/j.ijcard.2014.03.008
34. Plonsey R, Barr RC (1988) Extracellular fields. In: Bioelectricity. Springer, Boston, USA, p.149–163. https://doi.org/10.1007/978-1-4757-9456-4_7
35. Ivanushkina NG, Ivanko KO, Shpotak MO et al (2022) Reconstruction of action potentials of cardiac cells from extracellular field potentials. Radioelectron Commun Syst 65(7):354–364. https://doi.org/10.3103/S0735272722090047
36. Govoni M, Muscari C, Guarnieri C et al (2013) Mechanostimulation protocols for cardiac tissue engineering. Biomed Res Int 2013:918640. https://doi.org/10.1155/2013/918640
37. Morgan KY, Black LD (2017) Investigation into the effects of varying frequency of mechanical stimulation in a cycle-by-cycle

manner on engineered cardiac construct function. J Tissue Eng Regen Med 11(2):342–353. https://doi.org/10.1002/term.1915
38. Hülsmann J, Aubin H, Kranz A et al (2013) A novel customizable modular bioreactor system for whole-heart cultivation under controlled 3D biomechanical stimulation. J Artif Organs 16(3):294–304. https://doi.org/10.1007/s10047-013-0705-5
39. Akhyari P, Fedak PWM, Weisel RD et al (2002) Mechanical stretch regimen enhances the formation of bioengineered autologous cardiac muscle grafts. Circulation 106(12_suppl_1):I-137–I-142. https://doi.org/10.1161/01.cir.0000032893.55215.fc
40. Tulloch NL, Muskheli V, Razumova MV et al (2011) Growth of engineered human myocardium with mechanical loading and vascular coculture. Circ Res 109(1):47–59. https://doi.org/10.1161/CIRCRESAHA.110.237206
41. Kroll K, Chabria M, Wang K et al (2017) Electro-mechanical conditioning of human iPSC-derived cardiomyocytes for translational research. Prog Biophys Mol Biol 130(Pt B):212–222. https://doi.org/10.1016/j.pbiomolbio.2017.07.003
42. Miklas JW, Nunes SS, Sofla A et al (2014) Bioreactor for modulation of cardiac microtissue phenotype by combined static stretch and electrical stimulation. Biofabrication 6(2):024113. https://doi.org/10.1088/1758-5082/6/2/024113
43. Lu K, Seidel T, Cao-Ehlker X et al (2021) Progressive stretch enhances growth and maturation of 3D stem-cell-derived myocardium. Theranostics 11(13):6138–6153. https://doi.org/10.7150/thno.54999
44. Wang B, Wang GJ, To F et al (2013) Myocardial scaffold-based cardiac tissue engineering: application of coordinated mechanical and electrical stimulations. Langmuir 29(35):11109–11117. https://doi.org/10.1021/la401702w
45. Morgan KY, Black LD (2014) Mimicking isovolumic contraction with combined electromechanical stimulation improves the development of engineered cardiac constructs. Tissue Eng Part A 20(11–12):1654–1667. https://doi.org/10.1089/ten.TEA.2013.0355
46. Bootman MD, Higazi DR, Coombes S et al (2006) Calcium signalling during excitation-contraction coupling in mammalian atrial myocytes. J Cell Sci 119(Pt 19):3915–3925. https://doi.org/10.1242/jcs.03223
47. Korhonen T, Rapila R, Tavi P (2008) Mathematical model of mouse embryonic cardiomyocyte excitation-contraction coupling. J Gen Physiol 132(4):407–419. https://doi.org/10.1085/jgp.200809961
48. Garidel P, Schott H (2006) Fourier-transform midinfrared spectroscopy for analysis and screening of liquid protein formulations. Part 2: detailed analysis and applications. Bioprocess Int 4:48–55
49. Bastos MB, Burkhoff D, Maly J et al (2020) Invasive left ventricle pressure-volume analysis: overview and practical clinical implications. Eur Heart J 41(12):1286–1297. https://doi.org/10.1093/eurheartj/ehz552
50. Guyton AC, Hall JE (2011) Textbook of Medical Physiology (12th Ed.). Elsevier, Philadelphia, USA, p.45–103
51. Rangarajan S, Madden L, Bursac N (2014) Use of flow, electrical, and mechanical stimulation to promote engineering of striated muscles. Ann Biomed Eng 42(7):1391–1405. https://doi.org/10.1007/s10439-013-0966-4
52. Tandon N, Cannizzaro C, Chao PG et al (2009) Electrical stimulation systems for cardiac tissue engineering. Nat Protoc 4(2):155–173. https://doi.org/10.1038/nprot.2008.183
53. Santoni SM, Winston T, Hoang P et al (2018) Microsystems for electromechanical stimulations to engineered cardiac tissues. Microphysiol Syst 2:11. https://doi.org/10.21037/mps.2018.11.01
54. Lasher RA, Pahnke AQ, Johnson JM et al (2012) Electrical stimulation directs engineered cardiac tissue to an age-matched native phenotype. J Tissue Eng 3(1):2041731412455354. https://doi.org/10.1177/2041731412455354
55. Jameson JL, Fauci AS, Kasper DL et al (2018) Harrison's Manual of Medicine (20th Ed.). McGraw Hill Medical
56. Hagiwara Y, Hattori K, Aoki T et al (2011) Autofluorescence assessment of extracellular matrices of a cartilage-like tissue construct using a fluorescent image analyser. J Tissue Eng Regen Med 5(2):163–168. https://doi.org/10.1002/term.320
57. Silverthorn DU (2015) Human Physiology: an Integrated Approach (7th Ed.). Pearson
58. Gupta S, Sharma A, Archana S et al (2021) Mesenchymal stem cells for cardiac regeneration: from differentiation to cell delivery. Stem Cell Rev Rep 17(5):1666–1694. https://doi.org/10.1007/s12015-021-10168-0
59. Halim A, Ariyanti AD, Luo Q et al (2020) Recent progress in engineering mesenchymal stem cell differentiation. Stem Cell Rev Rep 16(4):661–674. https://doi.org/10.1007/s12015-020-09979-4
60. Huang Y, Zheng LS, Gong XH et al (2012) Effect of cyclic strain on cardiomyogenic differentiation of rat bone marrow derived mesenchymal stem cells. PLoS ONE 7(4):e34960. https://doi.org/10.1371/journal.pone.0034960
61. Li XH, Yu XY, Lin QX et al (2007) Bone marrow mesenchymal stem cells differentiate into functional cardiac phenotypes by cardiac microenvironment. J Mol Cell Cardiol 42(2):295–303. https://doi.org/10.1016/j.yjmcc.2006.07.002
62. Crameri RM, Aagaard P, Qvortrup K et al (2007) Myofibre damage in human skeletal muscle: effects of electrical stimulation versus voluntary contraction. J Physiol 583(Pt 1):365–380. https://doi.org/10.1113/jphysiol.2007.128827
63. Nosaka K, Aldayel A, Jubeau M et al (2011) Muscle damage induced by electrical stimulation. Eur J Appl Physiol 111(10):2427–2437. https://doi.org/10.1007/s00421-011-2086-x
64. Bachmann L, Diebolder R, Hibst R et al (2005) Changes in chemical composition and collagen structure of dentine tissue after erbium laser irradiation. Spectrochim Acta A Mol Biomol Spectrosc 61(11–12):2634–2639. https://doi.org/10.1016/j.saa.2004.09.026
65. Silva ZS Jr, Botta SB, Ana PA et al (2015) Effect of papain-based gel on type I collagen: spectroscopy applied for microstructural analysis. Sci Rep 5:11448. https://doi.org/10.1038/srep11448